PROCEEDINGS OF SCIENCE

AdS/CFT Correspondence for Scalar Field Theory in Lattice AdS_3

Cameron V. Cogburn,[a,*] **Richard C. Brower**[a,b] **and Evan Owen**[a]

[a] *Department of Physics, Boston University, 590 Commonwealth Avenue, Boston, MA 02215, USA*

[b] *Center for Computational Science, Boston University, 3 Cummington Mall, Boston, MA 02215, USA*

E-mail: cogburn@bu.edu, brower@bu.edu, ekowen@bu.edu

We use a regular tessellation of AdS_2 based on the $(2,3,7)$ triangle group, with an extension to Euclidean AdS_3, to study the AdS/CFT correspondence. Perturbative calculations are verified and Monte Carlo calculations for non-perturbative ϕ^4 theory exhibit critical phenomena.

The 38th International Symposium on Lattice Field Theory, LATTICE2021 26th-30th July, 2021 Zoom/Gather@Massachusetts Institute of Technology

*Speaker

1. Introduction

The study of strongly-coupled Quantum Field Theories (QFTs) is difficult, even before putting them in anti de-Sitter (AdS) space. The best developed numerical tool we have for studying strongly-coupled QFTs at the moment is lattice field theory. In [1] we constructed the basic lattice scaffolding to do non-perturbative calculations in AdS, with an explicit construction of and calculations done in AdS$_2$. In this work we extend these ideas to AdS$_3$.

The reasons to study strongly-coupled QFTs in AdS$_3$ are manifold. First, in the holographic correspondence the boundary theory of AdS$_3$ is the special case of CFT$_2$, for which there is a plethora of knowledge, examples, and analytic control of. Second, three dimensions is the minimum dimensionality needed to study non-trivial pure gravity. Finally, understanding AdS$_3$ in Minkowski space can help us understand the time evolution of simple quantum systems. This allows a connection with quantum computing, which requires unitary time evolution, as well as recently proposed hyperbolic lattice systems [2].

In this work we detail a lattice realization of AdS$_3$ amenable to study of all three of the preceding points. This talk is organized as follows. In Section 2 we detail our precise lattice construction of AdS$_3$. Section 3 focuses on the free theory, where we compute various propagators directly to compare the lattice to the continuum and as a check of our Monte Carlo. Section 4 then uses Monte Carlo methods to find the critical point in ϕ^4 theory. We finish in Section 5 with a discussion.

2. Lattice AdS$_3$

We begin with a discussion about AdS$_3$ and then its latticization. Ultimately our motivation is to be able to study non-perturbative aspects of QFTs in a fixed AdS background. The importance of this setup was pointed out long ago by [3], who showed a space with negative curvature acts as a natural bulk IR regulator.[1]

It is useful to choose a foliation of spacetime that best highlights the symmetries of the problem. We therefore work in Euclidean AdS$_3$ described by global coordinates with the induced metric

$$ds^2 = \ell^2(\cosh^2\rho\, d\tau^2 + d\rho^2 + \sinh^2\rho\, d\theta^2)\ , \tag{2.1}$$

where $\tau \in (-\infty, \infty)$, $\rho \in [0, \infty)$, and $\theta \in [0, 2\pi)$. This specific choice of coordinates makes manifest several unique properties of AdS$_3$ useful for the study of strongly-coupled systems.

First, the metric (2.1) is block diagonal in time and the hyperbolic plane $\mathbb{H}^2$,

$$ds^2 = g_{00}(x)d\tau^2 + ds^2_{\mathbb{H}^2}\ , \tag{2.2}$$

meaning the space is topologically a cylinder, $\mathbb{R} \times \mathbb{S}^2$. The conformal boundary is simply the boundary of the cylinder, a two-dimensional flat spacetime on which a putative CFT$_2$ could live, with all the tools and results that come with it. A visualization of AdS$_3$ spacetime is shown in Fig. 1.

The cylindrical topology also makes clear the time translation symmetry.[2] Since the dilatation generator $D = -\partial_\tau$ is the Hamiltonian conjugate to the global time, global coordinates are natural

[1]Through the UV/IR correspondence this is the same as a UV regulator on the boundary.
[2]As well as $SO(2)$ symmetry.

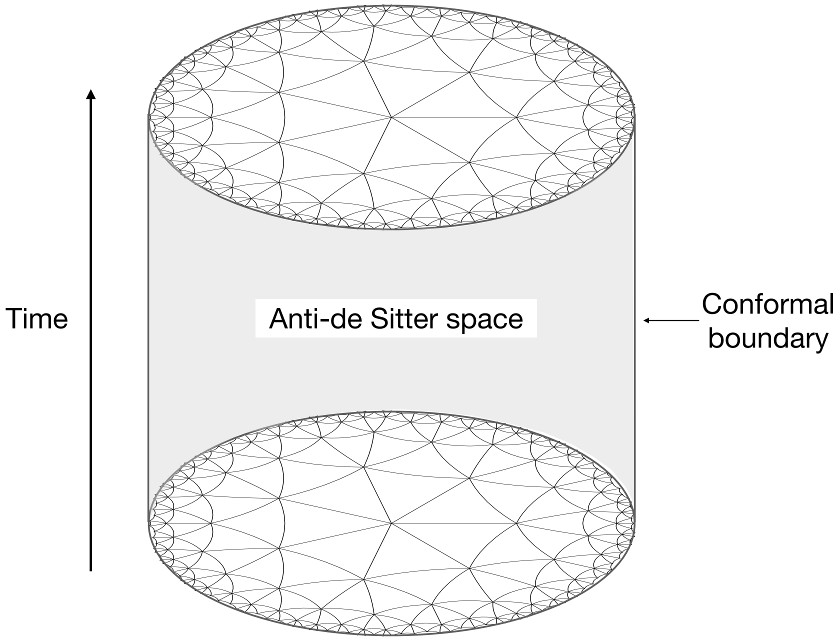

Figure 1: AdS$_3$ spacetime looks like a solid cylinder. At fixed time the space is the hyperbolic disk, which can be tessellated using equilateral hyperbolic triangles. Here, $(2, 3, 7)$ triangles are used.

for the study of dynamics. This allows a natural extension to AdS$_3$ of the lattice realization for $\mathbb{H}^2$ detailed in [1] using equilateral hyperbolic triangles via the triangle group. Concretely, we can extend the tessellated $\mathbb{H}^2$ into a latticized AdS$_3$ by tessellating $\mathbb{H}^2$ as before but at fixed t: $\phi(t,x) \longrightarrow \phi_i(t)$.[3]

In this note we are specifically interested in ϕ^4 theory given by the action

$$S = \frac{1}{2}\int dt \int d^2x\sqrt{g}(g^{\mu\nu}\partial_\mu\phi\partial_\nu\phi + m^2\phi^2 + \lambda\phi^4) \; , \tag{2.3}$$

where $\lambda = 0$ is the solvable free theory, and $\lambda \neq 0$ is the interacting theory. The resulting discretized action is then

$$S = \frac{1}{2}\int dt\Big[\sum_{j \text{ adj. to } i} \frac{\cosh\rho_i}{2} K_{ij}(\phi_i - \phi_j)^2 + \sum_i \sqrt{g_i}\cosh\rho_i(g_i^{00}(\partial_t\phi_i)^2 + m^2\phi_i^2 + \lambda\phi_i^4)\Big] \; , \tag{2.4}$$

with $\sqrt{g} = \cosh\rho_i\sqrt{g_i}$ and $g^{00} = 1/\cosh^2\rho_i$. The coefficients $\sqrt{g_i}$ and K_{ij} can be determined using the finite element method (FEM) [5]. This method sets the measure $\sqrt{g_i}$ to the volume at the dual sites, and the kinetic weights K_{ij} to the ratio S_{ij}/l_{ij} of the dual to the link (the Hodge start of the link l^*_{ij}) divided by the link l_{ij}.

To discretize time in the action (2.4) we introduce a lattice time with spacing $\Delta t = a_t$. The Euclidean lattice action on AdS$_3$ is then

$$S = a_t \sum_{i,t}\left(\frac{\sqrt{g_i}}{\cosh\rho_i}(\phi_{t,i} - \phi_{t+1,i})^2 + \cosh\rho_i L_{\mathbb{H}^2}[\phi_{t,i}]\right) \; . \tag{2.5}$$

[3]For a complementary way to latticize AdS$_3$ using a regular tessellation of hyperbolic 3-space see Ref. [4].

Here time t is treated as a lattice integer with the $\mathbb{H}^2$ Lagrangian given by

$$L_{\mathbb{H}^2}[\phi_{t,i}] = \frac{1}{2}\sum_{j \text{ adj. to } i} \frac{1}{2}K_{ij}(\phi_{t,i} - \phi_{t,j})^2 + \frac{1}{2}\sum_i \sqrt{g_i}(m^2\phi_i^2 + \lambda\phi_i^4)\ . \tag{2.6}$$

Expanding this out gives

$$S = \frac{a_t}{2}\left[\sum_{i,t}\sqrt{g_i}\frac{(\phi_{t,i} - \phi_{t+1,i})^2}{a_t^2\cosh\rho_i} + \cosh\rho_i\left(\sum_{j \text{ adj. to } i}\frac{1}{2}K_{ij}(\phi_{t,i} - \phi_{t,j})^2 + \sqrt{g_i}(m^2\phi_i^2 + \lambda\phi_i^4)\right)\right]\ . \tag{2.7}$$

It is important to note that because of the relative $\cosh\rho_i$ factors in (2.7) the lattice weights are not constant and are position dependent. Classically this comes from the $\cosh^2\rho\, d\tau^2$ term in the metric (2.1) that indicates that there is a gravitational force pushing particles towards the center in this foliation due to the increased energy cost needed to move radially outwards.

2.1 Lattice simulations

Before we can perform lattice simulations and measurements, we need to pick an explicit lattice for the discretized action (2.7). Given the separated form of (2.7), we latticize $\mathbb{H}^2$ using $(2,3,7)$ equilateral triangles as in [1], while keeping regular lattice time spacings a_t.

Because the lattice is a simple extension of the lattice realization for $\mathbb{H}^2$ detailed in [1], it is worth briefly reviewing the 2d construction. Here the hyperbolic disk can be tessellated using $(2,3,q)$ equilateral hyperbolic triangles.[4] Using hyperbolic triangles, an exponential growth in the number of points on the lattice boundary vs the total number of points is seen, as one would expect from holography. Given this tessellation, the lattice weights $\sqrt{g_i}$ and K_{ij} are

$$\sqrt{g_i} = \frac{q}{3}A_\Delta\,, \qquad K_{ij} = \frac{4A_\Delta}{3a^2}\,, \tag{2.8}$$

where the equilateral triangle area $A_\Delta = (\pi - 6\pi/q)\ell^2$ with side length a given by

$$\cosh(a/2\ell) = \frac{\cos(\pi/3)}{\sin(\pi/q)} = \frac{1}{2\sin(\pi/q)}\ . \tag{2.9}$$

There are two things to note. First, the 2d lattice weights (2.8) are constant and independent of position. This means we can ignore things like counterterms if interactions are turned on, as the counterterms are uniform just contributed an overall factor that falls out in any observable. Second, the triangle side length a is of order the AdS radius ℓ. Although this might suggest refinement is necessary to get sensible short-distance measurements, it was shown in [1] that excellent propagators can be obtained without refinement.

Given the AdS$_3$ lattice is a simple extension of the disk lattice, it shares many of the same properties, but also has important differences. Foremost, it shares the same exponential growth in points moving radially towards the boundary, again as expected from holography. However, a crucial difference is the lattice weights are now not constant and are position dependent, as discussed

[4] The choice $(2,3,7)$ is used as the top and bottom of the cylinder in Fig. 1.

below Eq. (2.7). A consequence of this is that traversing radially on the lattice towards the boundary, the time direction becomes more heavily skewed. This makes probing the boundary theory a subtle task.

In practice we can alter this skew through the ratio $\frac{a}{a_t}$, which determines how skewed the temporal direction is relative to the spatial direction. Because we are interested in bulk physics in this work we take $\frac{a}{a_t} = 1$ in our code. If we were interested in the critical boundary theory it would be worth exploring changing this ratio to produce a regular ratio of points on the approach to the lattice boundary. We save this for future work.

In practice the lattice is constructed similarly to the 2d case, except now there are N_t time slices in addition to the L spatial layers, as well as different weights, discussed previously. Fields ϕ_i are placed on interior vertices labeled by (τ_i, r_i, θ_i). Dirichlet boundary conditions are imposed on a fictitious $(L+1)$-th layer whereas periodic boundary conditions are taken temporally. To avoid boundary effects, the L-th layer is not included in measurements.

3. The Free Theory

In this section we study the free discretized theory in AdS_3, given by (2.7) with $\lambda = 0$. The continuum limit is analytically known and allows us to check our lattice construction and Monte Carlo methods.

We focus on the bulk-bulk propagator for both theoretical and practical reasons. The theoretical reason is that all other propagators (the bulk-boundary and boundary-boundary two-point functions) can be extracted from the bulk Green's function. The practical reason is that finite lattices never truly reach infinity so all propagators are inherently bulk-bulk propagators on the lattice.

3.1 Propagators

For a given mass-squared m^2, the analytic bulk Green's function $G_{bb}(X, X')$ between two points X and X' in AdS_{d+1} is the solution to the equation

$$(-\nabla^2 + m^2)G = \frac{1}{\sqrt{g}}\delta^{d+1}(X - X') \ . \tag{3.1}$$

Here ∇_μ is the covariant derivative, the Laplace operator $\nabla^2 = \nabla_\mu \nabla^\mu = \frac{1}{\sqrt{g}}\partial_\mu \sqrt{g} g^{\mu\nu}\partial_\nu$ and $\frac{1}{\sqrt{g}}\delta^{d+1}(X - X')$ is defined as the δ-function for AdS_{d+1}. The Green's function is given by [6, 7]

$$G_{bb}(X, X') = G_{bb}(\sigma) = e^{-\Delta\sigma}{}_2F_1\left(\Delta, \frac{d}{2}, \Delta + 1 - \frac{d}{2}; e^{-2\sigma}\right) , \tag{3.2}$$

where σ is the geodesic between X and X' and the scaling dimension is related to the mass through $m^2\ell^2 = \Delta(\Delta - d)$ with ℓ being the AdS radius. For $d = 2$ the bulk Green's function is given by

$$G_{bb}(\sigma) = \frac{e^{-\Delta\sigma}}{1 - e^{-2\sigma}} \tag{3.3}$$

with the geodesic distance given by

$$\cosh(\sigma) = \cosh(t - t')\cosh(\rho)\cosh(\rho') - \sinh(\rho)\sinh(\rho')\cos(\theta - \theta') \tag{3.4}$$

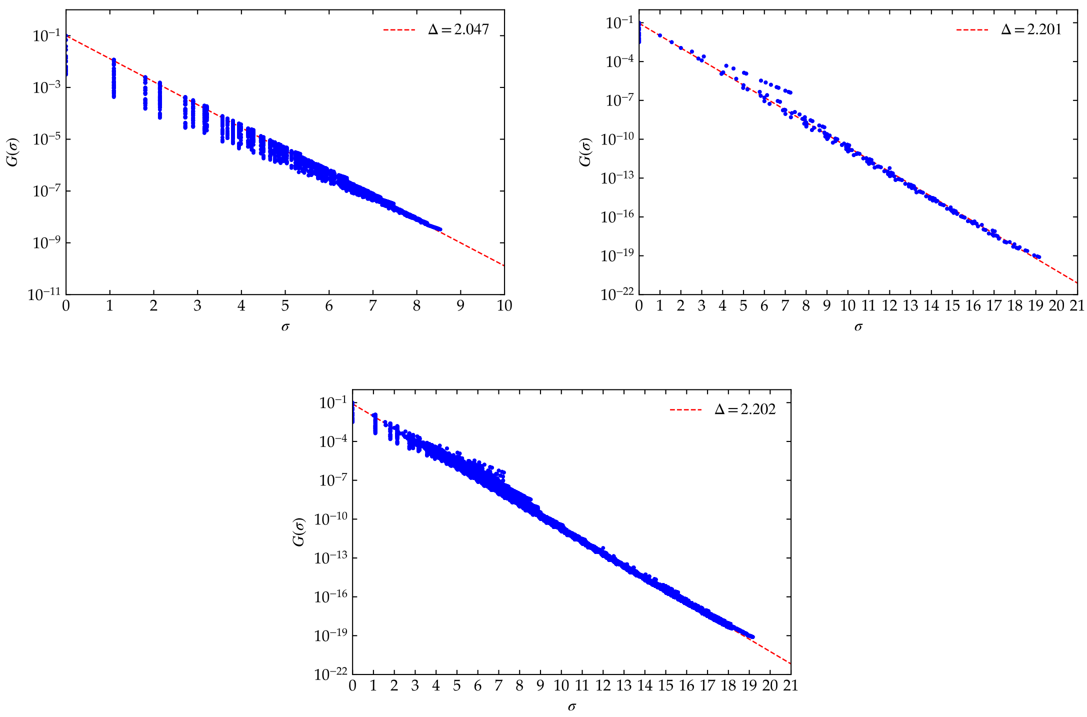

Figure 2: Checks in the perturbative regime of the AdS$_3$ lattice realization from a direct inversion of the massless Green's function equation for $L = 4$. *Top left:* The all-to-all spatial propagator for $t = 0$. *Top right:* The all-to-all temporal propagator for the center point. *Bottom:* All-to-all propagator.

in global hyperbolic coordinates (2.1). The discretized form of the Green's function equation (3.1) is given by

$$(-\nabla^2_{ij} + \delta_{ij} m^2) G_{ij} = \frac{1}{\cosh \rho_i \sqrt{g_i}} \delta^{d+1}_{ij}(X - X') \ . \tag{3.5}$$

For the massless case we check the lattice propagator G_{ij} against the analytic one G_{bb} by taking all points to all other points, as well as taking the center point and looking at the propagator to all other spatial points or back to itself over all times. Fig. 2 shows the results of this comparison; we see there is good agreement. We note that similar to [4], the scaling dimension Δ_{all} is slightly larger than the continuum value $\Delta = 2$.

At the boundary Eq. (3.3) reduces to the boundary propagator

$$\ln G_{\partial\partial} \propto -\Delta \ln(1 - \cos\theta) \ , \tag{3.6}$$

offering another check for the lattice propagators. In practice by "boundary" we mean points on the $L - 1$ layer of the lattice. Essentially we are checking mass-scaling dimension relation $m^2\ell^2 = \Delta(\Delta - 2)$ from holography. The results are shown in Fig. 2 and show good agreement with the expected value of $\Delta = 2$ for the massless case.

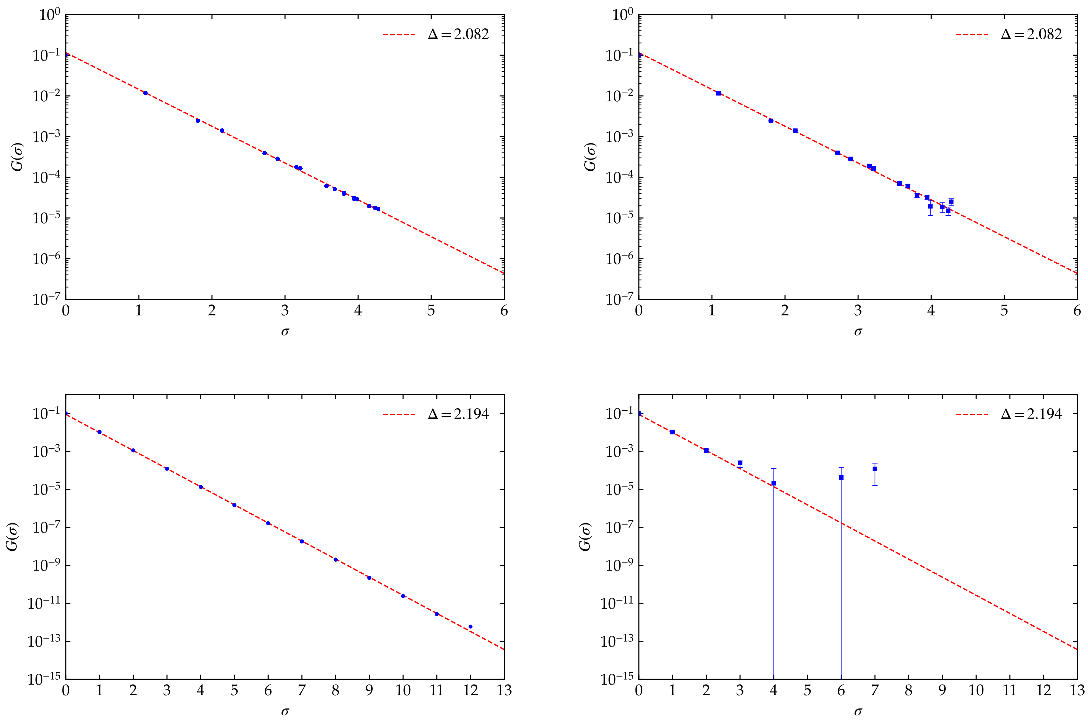

Figure 3: Checks between the direct inversion (*left*) and Monte Carlo (*right*) for propagators for the massless case with $L = 4$. *Top:* Propagator from the center point to all other spatial points on the disk. *Right:* Propagator from the center point to all other temporal center points.

4. The interacting theory

To go beyond the free theory of Section 3 we look at the action (2.7) with $\lambda \neq 0$. Including interactions necessitates the use of Monte Carlo methods to evaluate the Euclidean path integral. We are specifically interested in seeing if our lattice supports a critical point. This is the first step in being able to eventually answer questions such as what type of CFT is produced on the boundary at criticality.

Whether or not there is a critical point is of itself an interesting question, though. It is unclear, a priori, if there is even a critical point as a parametrically large number of lattice points live on the boundary as the number of layers increase. The choice of lattice equilateral triangles $(2, 3, q)$ likely influences the results as it determines the ratio of the total number of points that live on the lattice boundary. Ref. [8] looked at the Ising model in $\mathbb{H}^3$ using a $\{5,3,5\}$ lattice with periodic boundary conditions and found results consistent with mean field theory for the magnetic susceptibility critical exponent γ.

As a first step towards future work, we present evidence of a critical point for our lattice detailed above.

4.1 The ϕ^4 critical point

To study the theory (2.7) with non-zero λ and tachyonic mass $\mu^2 = -m^2$, we perform a lattice Monte Carlo simulation using a combination of Metropolis [10] and overrelaxation [11] updates. The critical point will depend on the two parameters λ and μ^2, so we set $\lambda = 2$ and sweep over μ^2 values until we find the critical μ_c^2, and do this for an increasing number of lattice layers.[5] For each combined lattice layer we choose the number of time slices N_t to be equal to the number of points on the outermost spatial layer L, so that the lattice boundary has N_t^2 points.

We look for two common features to determine the critical point: the divergence of the magnetic susceptibility, and the approach to a step function of the Binder cumulant [12]. The magnetic susceptibility χ is defined as

$$\chi = \langle m^2 \rangle - \langle |m| \rangle^2 \,, \tag{4.1}$$

where we have introduced $m = \sum_i \sqrt{g_i}\phi_i$ as the magnetization. Because of the expected divergence near the critical point we include a number of Wolff cluster updates [13] to achieve good statistics. As shown in Fig. 4, we find a clear peak in the susceptibility that grows with additional lattice layers, consistent with a second-order phase transition.

Next we look at the 4th Binder cumulant U_4, defined as

$$U_4 = \frac{3}{2}\left(1 - \frac{\langle m^4 \rangle}{3\langle m^2 \rangle}\right) \,. \tag{4.2}$$

As seen in Fig. 4, U_4 remains constant at μ_c^2 as the number of layers is increased, offering further evidence of a second-order phase transition for ϕ^4 theory on this lattice.

We defer to a later work in providing the critical exponents from a finite scaling analysis as there are a number of subtleties in approaching the boundary inherent in this lattice realization that need to be accounted for properly to be able to extract accurate exponents.[6]

[5] We plot as a function of the reduced temperature, $t = (\mu^2 - \mu_c^2)/\mu_c^2$, where we define the critical mass μ_c^2 as the value of the mass where the peak susceptibility occurs. This allows a clear comparison of the divergence as a function of the number of layers.

[6] For example, defining a system length scale, taking into account the exact boundary conditions, and having a non-uniform boundary.

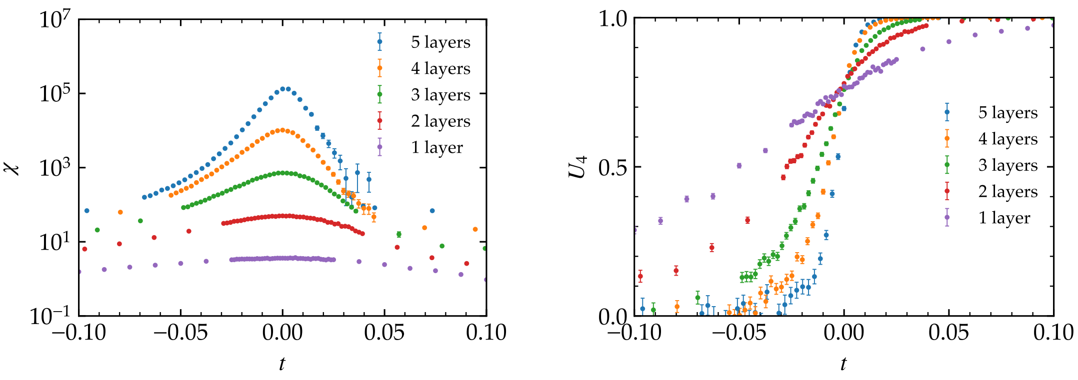

Figure 4: Evidence for a second order phase transition for bulk ϕ^4 theory in the Euclidean AdS$_3$ cylinder at $\lambda = 2$. *Left:* The divergence of the magnetic susceptibility at the critical point as layers are added. *Right:* The sharpening of the transition of the Binder cumulant from zero to one as layers are added. Both are plotted as a function of the reduced temperature, $t = (\mu^2 - \mu_c^2)/\mu_c^2$, where the critical mass μ_c^2 is the value of the mass where the peak susceptibility occurs.

5. Discussion

In this talk we have detailed a lattice realization of the Euclidean cylinder foliation of AdS$_3$ spacetime utilizing equilateral triangles based on the triangle group and time translation symmetry suitable for the study of non-perturbative phenomena in the AdS$_3$/CFT$_2$ correspondence. Checks of the free theory propagators using direct inversion as well as Monte Carlo agree with the expected continuum results. By looking at the magnetic susceptibility and the Binder cumulant we find strong evidence that this construction supports a critical point for ϕ^4 theory. Further work understanding the subtleties of approaching the boundary will be needed to accurately determine the scaling exponents as well as if the boundary theory is a short- or long-range Ising model, or something else. Characterizing the boundary will help answer the question of whether the critical behavior is confined to just the bulk or both the bulk and the boundary.

Acknowledgements

This work was supported by the U.S. Department of Energy (DOE) under Award No. DE-SC0019139 for C.V.C. and E.K.O., and Award No. DE-SC0015845 for R.C.B.

References

[1] R. C. Brower, C. V. Cogburn, A. L. Fitzpatrick, D. Howarth, and C.-I. Tan, "Lattice Setup for Quantum Field Theory in AdS$_2$," arXiv:1912.07606 [hep-th].

[2] A. J. Kollár, M. Fitzpatrick, and A. A. Houck, "Hyperbolic lattices in circuit quantum electrodynamics," *Nature* **571** no. 7763, (Jul, 2019) 45–50. http://dx.doi.org/10.1038/s41586-019-1348-3.

[3] C. G. Callan, Jr. and F. Wilczek, "INFRARED BEHAVIOR AT NEGATIVE CURVATURE," *Nucl. Phys. B* **340** (1990) 366–386.

[4] M. Asaduzzaman, S. Catterall, J. Hubisz, R. Nelson, and J. Unmuth-Yockey, "Holography on tessellations of hyperbolic space," *Physical Review D* **102** no. 3, (Aug, 2020) . http://dx.doi.org/10.1103/PhysRevD.102.034511.

[5] G. Strang and G. Fix, *An Analysis of the Finite Element Method 2nd Edition*. Wellesley-Cambridge, 2nd ed., 5, 2008. http://amazon.com/o/ASIN/0980232708/.

[6] C. P. Burgess and C. A. Lutken, "Propagators and Effective Potentials in Anti-de Sitter Space," *Phys. Lett. B* **153** (1985) 137–141.

[7] E. Hijano, P. Kraus, E. Perlmutter, and R. Snively, "Witten Diagrams Revisited: The AdS Geometry of Conformal Blocks," *JHEP* **01** (2016) 146, arXiv:1508.00501 [hep-th].

[8] N. P. Breuckmann, B. Placke, and A. Roy, "Critical properties of the ising model in hyperbolic space," *Physical Review E* **101** no. 2, (Feb, 2020) . http://dx.doi.org/10.1103/PhysRevE.101.022124.

[9] A. J. Kóllar, M. Fitzpatrick, and A. A. Houck, "Hyperbolic lattices in circuit quantum electrodynamics," *Nature* **571** no. 7763, (Jul 4, 2019) 45–50.

[10] N. Metropolis, A. Rosenbluth, M. Rosenbluth, A. Teller, E. Teller, "Equation of State Calculations by Fast Computing Machines," Journal of Chemical Physics. **21** 1087 (1953).

[11] S. L. Adler, "Over-relaxation method for the Monte Carlo evaluation of the partition function for multiquadratic actions," Phys. Rev. D **23**, 2901 (1981).

[12] K. Binder, "Finite size scaling analysis of ising model block distribution functions," in *Finite-Size Scaling*, J. L. CARDY, ed., vol. 2 of *Current Physics–Sources and Comments*, pp. 79–100. Elsevier, 1988. https://www.sciencedirect.com/science/article/pii/B9780444871091500121.

[13] U. Wolff, "Collective Monte Carlo Updating for Spin Systems," Phys. Rev. Lett. **62**, 361 (1989).